PDZ interactions regulate rapid turnover of the scaffolding protein EBP50 in microvilli

Damien Garbett and Anthony Bretscher

Department of Molecular Biology and Genetics, Weill Institute for Cell and Molecular Biology, Cornell University, Ithaca, NY 14853

Scaffolding proteins containing PDZ (postsynaptic density 95/discs large/zonula occludens-1) domains are believed to provide relatively stable linkages between components of macromolecular complexes and in some cases to bridge to the actin cytoskeleton. The microvillar scaffolding protein EBP50 (ERM-binding phosphoprotein of 50 kD), consisting of two PDZ domains and an ezrin-binding site, retains specific proteins in microvilli and is necessary for microvillar biogenesis. Our analysis of the dynamics of microvillar proteins in vivo indicated that ezrin and microvillar membrane proteins had dynamics consistent with actin treadmilling and microvillar lifetimes. However, EBP50 was highly dynamic, turning over within seconds. EBP50 turnover was reduced by mutations that inactivate its PDZ domains and was enhanced by protein kinase C phosphorylation. Using a novel in vitro photoactivation fluorescence assay, the EBP50–ezrin interaction was shown to have a slow off-rate that was dramatically enhanced in a PDZ-regulated manner by addition of cell extract to near in vivo levels. Thus, the linking of relatively stable microvillar components can be mediated by surprisingly dynamic EBP50, a finding that may have important ramifications for other scaffolding proteins.

Introduction

Scaffolding proteins containing PDZ (postsynaptic density 95/discs large/zona occludens-1) domains are often found at sites of macromolecular protein complexes, such as adherens and neuromuscular junctions (Romero et al., 2011). As the name implies, they are generally assumed to provide relatively stable connections linking functionally distinct proteins. The finding that the scaffolding protein EBP50 (ERM-binding phosphoprotein of 50 kD) is an essential component of microvilli present on cultured epithelial cells raised the question of how stable the components of microvilli are (Hanono et al., 2006).

The presence of microvilli on epithelial cells is dependent on members of the ERM (ezrin/radixin/moesin) protein family. These proteins consist of a membrane-associated N-terminal FERM (4.1 ERM) domain followed by an α-helical region and a C-terminal region that can bind either the FERM domain or F-actin (Fehon et al., 2010). This intramolecular association with the FERM domain creates a closed conformation in which both membrane and F-actin–binding sites are masked. Upon PIP$_2$ (phosphatidylinositol 4,5-bisphosphate) binding and phosphorylation of a conserved threonine residue (T567 in ezrin), the C-terminal domain is released to unmask the F-actin–binding site in the tail and ligand-binding sites on the FERM domain.

Thus, the activation of ezrin provides a regulated linkage between F-actin and membrane proteins as well as with EBP50 (Reczek and Bretscher, 1998).

EBP50, also known as NHERF1 (Na$^+$-H$^+$ exchanger regulatory factor 1), consists of two PDZ domains and a C-terminal ezrin-binding site. It was identified by its ability to bind to the FERM domain and also independently discovered as a factor necessary for conferring PKA regulation of NHE3 (Na$^+$-H$^+$ exchanger 3; Weinman et al., 1995; Reczek et al., 1997). EBP50 binds the ERM FERM domain with high affinity, which has been estimated to have a K_d of 1.7 nM (Terawaki et al., 2006). Since its discovery, EBP50 has been shown to bind multiple ligands through its two PDZ domains (Weinman et al., 2006). Recently, we showed that microvillar formation in cultured cells required EBP50—and, specifically, its ability to bind ezrin via its tail—and ligands through its PDZ1 domain (Garbett et al., 2010).

In this study, we analyze the dynamics of microvillar proteins in vivo. We find that membrane proteins and ezrin show similar dynamics consistent with rates of actin treadmilling and

The Rockefeller University Press $30.00
J. Cell Biol. Vol. 198 No. 2 195–203
www.jcb.org/cgi/doi/10.1083/jcb.201204008

JCB 195

Figure 1. **EBP50 undergoes rapid turnover in microvilli.** (A) FRAP of microvilli on the apical membrane of JEG-3 cells. The region marked by a green box was photobleached; the red box indicates the region shown in B. Bar, 5 µm. (B) Representative time points from photobleaching experiments of GFP-tagged EBP50, ezrin, TROP2, and PCX. Bars, 2 µm. (C) Recovery curves of GFP-EBP50 ($n = 13$), ezrin ($n = 19$), TROP2 ($n = 16$), and PCX ($n = 7$). Error bars show SD.
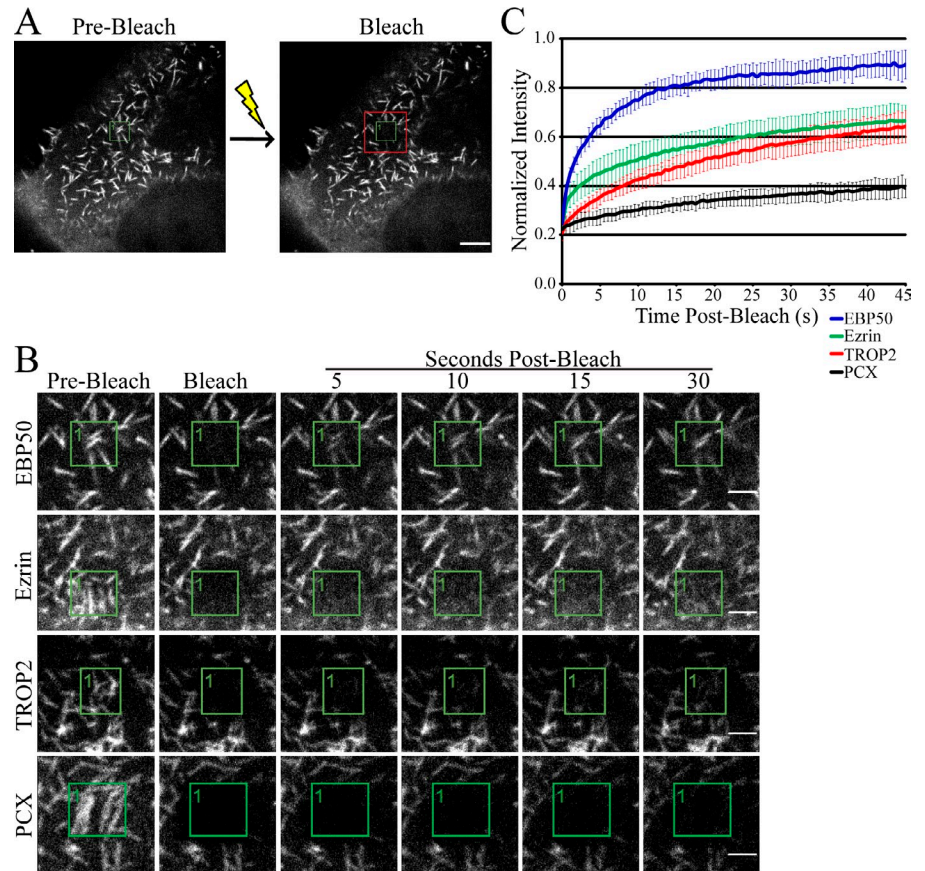
microvillar half-lives, whereas EBP50 is surprisingly dynamic. Remarkably, mutations that selectively inactivate EBP50's PDZ domains reduce its dynamics, whereas mutations mimicking PKC phosphorylation increase turnover. These results demonstrate an as of yet unexpected ability of a scaffolding protein to be highly dynamic and reveal that its dynamics can be modulated by binding PDZ ligands, which in turn influence the longevity of the EBP50–ezrin interaction.

Results and discussion

EBP50 is a highly dynamic component of microvilli

Microvilli on cultured cells are reported to have a lifetime of 12–15 min, as seen using scanning ion conductance microscopy (Gorelik et al., 2003). To see whether other techniques yield similar results, we explored the dynamics of microvilli by imaging expressed GFP-EBP50 or ezrin-GFP in JEG-3 cells, a choriocarcinoma-derived line that displays abundant microvilli on its apical surface. Although individual microvilli were difficult to track when densely packed, in areas where they were sparser, we found that microvilli had lifetimes in the 7–15-min time range (Fig. S1 A).

How might the dynamics of microvillar components relate to microvillar lifetimes? Brush border myosin I is relatively dynamic compared with actin, showing 80% recovery in about 1 min (Tyska and Mooseker, 2002; Waharte et al., 2005). We have suggested a model in which ezrin is activated by phosphorylation

at the microvillus tip and remains associated with treadmilling actin filaments until it is released at the microvillus base (Hanono et al., 2006). Actin treadmills at ∼0.2 µm/min (Loomis et al., 2003), so this model predicts that ezrin and tightly bound EBP50 will have lifetimes of several minutes in a 1-µm-long microvillus or about the half-life of a microvillus. Therefore, we used FRAP to estimate the dynamics of ezrin, EBP50, and several other microvillar components in vivo to see whether they fit this model.

We first determined the dynamics of the microvillar transmembrane protein TROP2-GFP, which binds to ezrin (unpublished data) and ezrin-GFP. For these experiments, each construct was expressed at a low level in JEG-3 cells and a small area bleached, and the recovery was then monitored. Experiments on multiple cells showed very reproducible recovery data (Fig. 1, A and C), which fit well to double exponential curves (Fig. S1 B). Both TROP2-GFP and ezrin-GFP recover slowly, with about half the microvillar fluorescence returning in 30 s (Fig. 1, B and C), which is consistent with what has been seen for ezrin by two-photon microscopy (Coscoy et al., 2002). As TROP2 is a transmembrane protein, its recovery is restricted to two dimensions, suggesting that ezrin is relatively firmly bound in the microvillus, as it has full access to the cytoplasm, which is consistent with our model. Surprisingly, GFP-EBP50 recovered very fast, within 5 s, showing that it is a highly dynamic component of microvilli (Fig. 1, B and C). This is very unexpected, as EBP50 binds active ezrin with a K_d in the nanomolar range, so it would be expected to have a very slow off-rate and therefore show similar dynamics to ezrin. It has been shown that
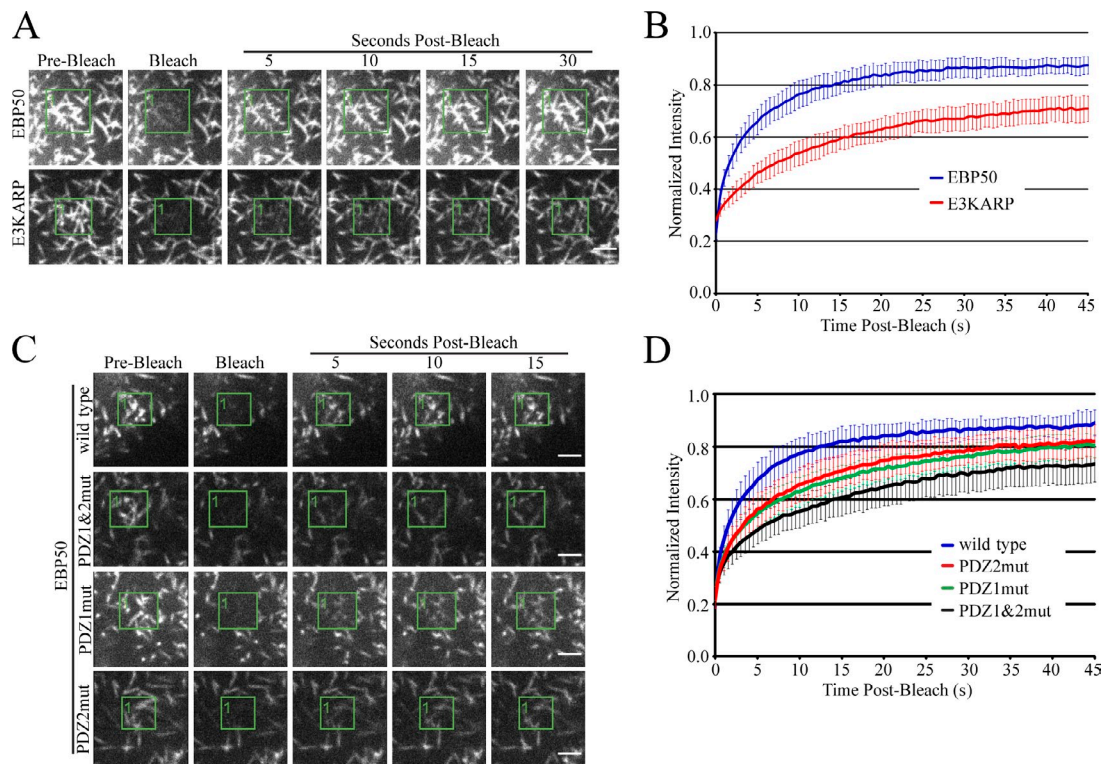
Figure 2. **EBP50's PDZ domains contribute to its rapid turnover.** (A) Time points from photobleaching of GFP-tagged EBP50 and E3KARP. Bars, 2 µm. (B) Recovery curves of GFP-EBP50 ($n = 18$) and E3KARP ($n = 11$). (C) Time points from photobleaching of GFP-EBP50 PDZ mutants (mut). Bars, 2 µm. (A and C) Photobleached regions are shown as green boxes. (D) Recovery curves of GFP-EBP50 wild type ($n = 18$), PDZ2 mutant ($n = 24$), PDZ1 mutant ($n = 24$), and PDZ1&2 mutant ($n = 21$). All error bars represent SD.

the membrane protein podocalyxin (PCX)/Gp135 localizes to microvilli in part through its C-terminal tail binding to the PDZ2 domain of EBP50 (Yu et al., 2007; Francis et al., 2011). Consistent with being restricted to the membrane, GFP-PCX is very stable in microvilli (Fig. 1, B and C). Thus, EBP50, which is necessary both for the assembly of microvilli on these cells and for retaining the localization of the membrane protein PCX to microvilli, is much more dynamic than both its cytoskeletal ligand ezrin and a transmembrane ligand.

PDZ binding is required for rapid EBP50 dynamics

Another member of the NHERF family, E3KARP (NHE3 kinase A regulatory protein), also binds ezrin with high affinity and has two PDZ domains highly conserved with those in EBP50. GFP-E3KARP is much less dynamic in microvilli than GFP-EBP50, indicating that, despite being closely related proteins, some distinct property of EBP50 renders it highly dynamic (Fig. 2, A and B).

We have shown that EBP50's function in microvillar formation requires its ability to both bind ezrin and retain a functional PDZ1 domain, whereas a functional PDZ2 domain is dispensable (Garbett et al., 2010). Ezrin binding is necessary to recruit EBP50 to microvilli, whereas functional PDZ domains are not when expressed in the context of endogenous EBP50 (unpublished data). This allows for us to assess the role of the PDZ domains on EBP50's dynamics; the simplest model would predict that mutations inactivating EBP50's PDZ domains should make it even more dynamic in vivo. Consistent with this prediction,

overexpression of parathyroid hormone receptor, a PDZ1 ligand, reduces EBP50 turnover at the basal plasma membrane in rat osteosarcoma cells (Ardura et al., 2011). To see whether this was also true in microvilli, EBP50's predominant physiological localization, we next examined the dynamics of GFP-EBP50 constructs containing inactivating mutations in PDZ1, PDZ2, and PDZ1&2. Surprisingly, mutating either PDZ1 or PDZ2 each slowed the dynamics of GFP-EBP50 recovery to a similar extent (Fig. 2, C and D). These effects were additive, as the PDZ1&2 double mutant recovered even slower, approaching recovery kinetics similar to that seen for ezrin-GFP (Fig. 2, C and D).

Photoactivation provides a powerful complementary tool to FRAP for directly selecting and monitoring the turnover of specific pools of proteins (Patterson and Lippincott-Schwartz, 2002; Lippincott-Schwartz and Patterson, 2009). Therefore, we examined the dynamics of EBP50 by using photoactivatable GFP (PAGFP). Cells were transfected to express both TagRFPT-EBP50 and PAGFP-EBP50. TagRFPT-EBP50 was used to select microvillar regions for analysis, and then a small area of PAGFP-EBP50 was activated, and its loss over time was recorded (Fig. 3 A). Using this system, EBP50 was again found to be highly dynamic, with the PAGFP-EBP50 signal being lost within seconds (Fig. 3, B and C). This approach was repeated using the PDZ1&2 double mutant as well as an EBP50 mutant to which a C-terminal alanine had been added (LA mutant), which weakens its ability to interact with ezrin (Fig. 3, B and C). All of the resulting photoactivation curves were highly reproducible and fit well to double exponential decay curves (Fig. 3, C and E).
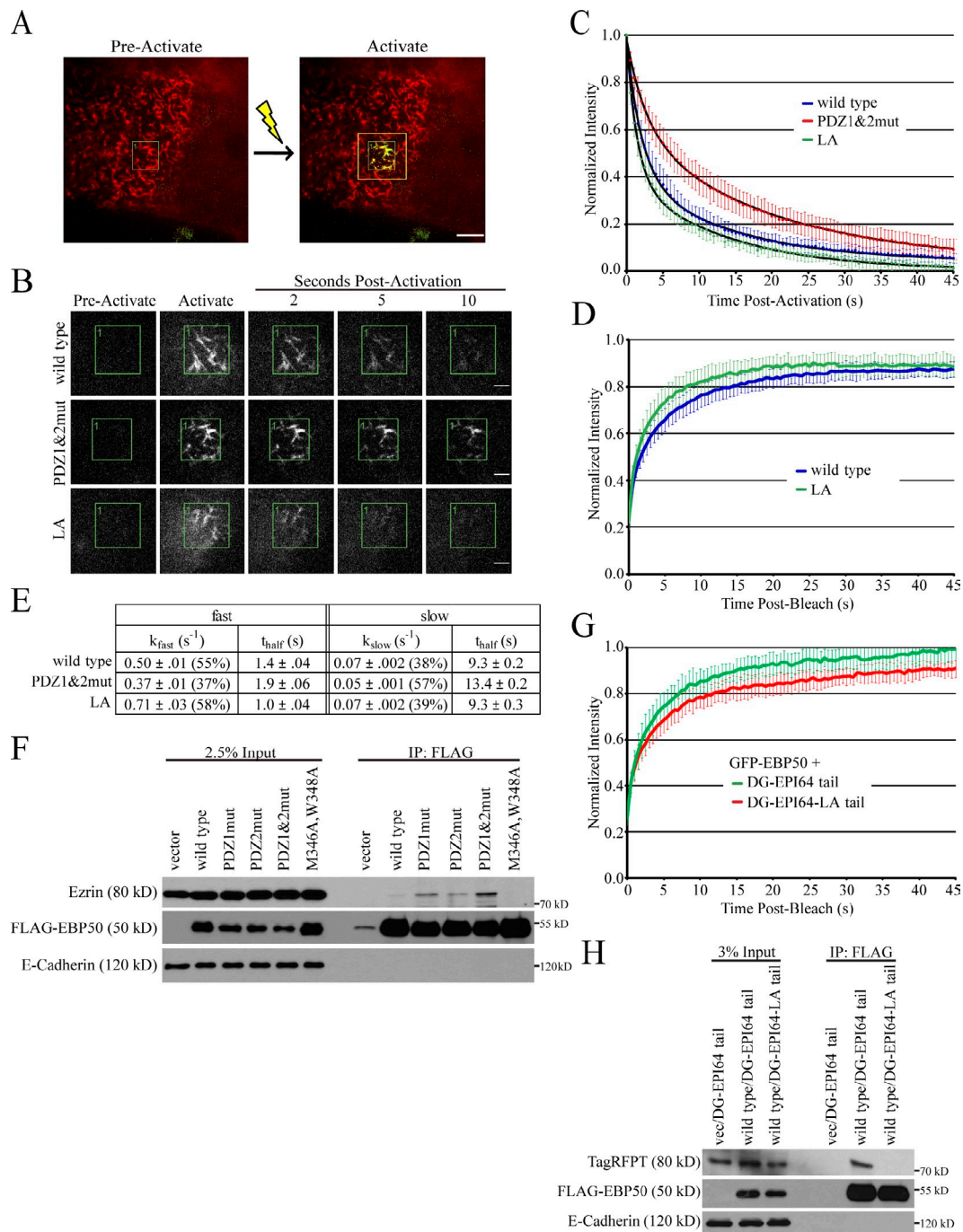
Figure 3. PDZ and ezrin binding both contribute to EBP50 dynamics. (A) Photoactivation of EBP50 in microvilli on JEG-3 cells. The region marked by a green box was photoactivated, and the yellow box indicates the region shown in B. Bar, 5 µm. (B) Time points from photoactivation of PAGFP-tagged EBP50 constructs. Bars, 2 µm. (C) Photoactivation decay curves of PAGFP-EBP50 wild type ($n = 16$), PDZ1&2 mutant (mut; $n = 17$), and LA mutant ($n = 12$; wild type vs. LA mutant, $P < 0.0001$). Black lines represent fitted curves with corresponding rates shown in E. (D) FRAP recovery curves of GFP-EBP50 wild type ($n = 18$) and LA mutant ($n = 19$; $P < 0.0001$). (E) Table of rates and half-lives of double exponential decay curve fits shown in C (±SD). (F) 3xFLAG-tagged EBP50 constructs expressed in JEG-3 cells were immunoprecipitated (IP) and blotted for FLAG, endogenous ezrin, and E-cadherin as a control. (G) FRAP recovery curves of GFP-EBP50 in cells coexpressing TagRFPT-tagged DG–EPI64 tail ($n = 8$) or DG-EPI64–LA tail ($n = 8$; $P < 0.0001$). (H) 3xFLAG-tagged EBP50 and TagRFPT-tagged DG–EPI64 tail or DG-EPI64–LA tail coexpressed in JEG-3 cells were immunoprecipitated and blotted for FLAG, TagRFPT, and E-cadherin as a control. vec, vector. All error bars represent SD.

Consistent with the FRAP results, the PDZ1&2 mutant reduced turnover significantly compared with wild type (Fig. 3, B, C, and E). The C-terminal EBP50 LA mutant showed a slight but significant increase in dynamics compared with wild-type EBP50, suggesting that weakening the interaction with ezrin increases

EBP50 turnover (Fig. 3, B–D). Thus, the combined FRAP and photoactivation data consistently show that EBP50 is highly dynamic in vivo, and this requires functional PDZ domains. This strongly suggests that EBP50's in vivo dynamics is influenced by proteins interacting with both of its two PDZ domains.

Although EBP50 binds the ezrin FERM domain tenaciously in vitro (Terawaki et al., 2006), we have been perplexed by the weak recovery of ezrin when EBP50 is immunoprecipitated out of JEG-3 cell extracts. To see whether this is related to EBP50's dynamics in vivo, we immunoprecipitated 3xFLAG-tagged wild-type EBP50 or its PDZ mutants that show reduced dynamics and blotted for endogenous ezrin (Fig. 3 F). Although ezrin is barely detectable in immunoprecipitates from wild-type EBP50–expressing cells, it is clearly visible in the single PDZ1 or PDZ2 mutants and most strongly with the PDZ1&2 double mutant and is not seen with the EBP50 M346A,W348A mutant defective in ezrin binding (Terawaki et al., 2006). Therefore, the dynamics seen for wild-type EBP50 in vivo is reflected by the inability of EBP50 and ezrin to form a stable immunoprecipitable complex.

To test whether PDZ ligands can stimulate increased EBP50 turnover, we generated a TagRFPT-tagged chimeric fusion, dystroglycan (DG)–EPI64 tail, of the microvillar protein β-DG fused to the C-terminal PDZ-binding tail of EPI64 (EBP50 PDZ interactor of 64 kD; Reczek and Bretscher, 2001; Spence et al., 2004). We expressed DG–EPI64 tail with GFP-EBP50 and performed photobleaching experiments on microvilli containing both constructs, as before. Indeed, DG–EPI64 tail, but not DG-EPI64–LA tail, a mutant with an additional C-terminal alanine added to block PDZ binding, was able to associate with EBP50 and increase its turnover in microvilli (Fig. 3, G and H), suggesting that interaction with EBP50's PDZ domains results in increased turnover, perhaps reflecting an enhanced dissociation from ezrin.

Phosphorylation by PKC enhances EBP50 turnover in microvilli

EBP50 can be phosphorylated by PKC on serines 162, 339, and 340 (Raghuram et al., 2003; Fouassier et al., 2005), and this inhibits its ability to bind to PDZ ligands simultaneously but has no effect on ezrin binding in vitro (Garbett et al., 2010). However, PKC phosphorylation has been shown to perturb the ezrin interaction, as seen by coimmunoprecipitation from cell lysates (Chen et al., 2012). To determine whether PKC phosphorylation increases turnover of EBP50, we performed photobleaching experiments of the phosphomimetic mutant GFP-EBP50-S162, 339,340D (PKCsD; Fig. 4). Indeed, EBP50-PKCsD showed modestly enhanced turnover compared with wild-type EBP50 and less association with ezrin in vivo (Fig. 4, A–C). To determine whether PKC phosphorylation was enhancing EBP50 turnover via promoting PDZ interactions, we mutated both PDZ domains in the PKC site–phosphomimetic EBP50 mutant (PKCsD-PDZ1&2mut) and found that both its microvillar turnover and ezrin binding were restored to wild-type levels (Fig. 4, A–C).

The stable ezrin–EBP50 interaction can be modulated in vitro

To begin a biochemical exploration of the aforementioned in vivo phenomena, we examined the interaction of EBP50 with ezrin in vitro. To estimate the off-rate of EBP50 from ezrin, ezrin FERM domain was covalently coupled to beads to give a concentration of 240 nM of bound protein, and then substoichiometric PAGFP-EBP50 was added at 40 nM to bind the coupled FERM domain. After a quick wash, the beads were placed in 1 µM
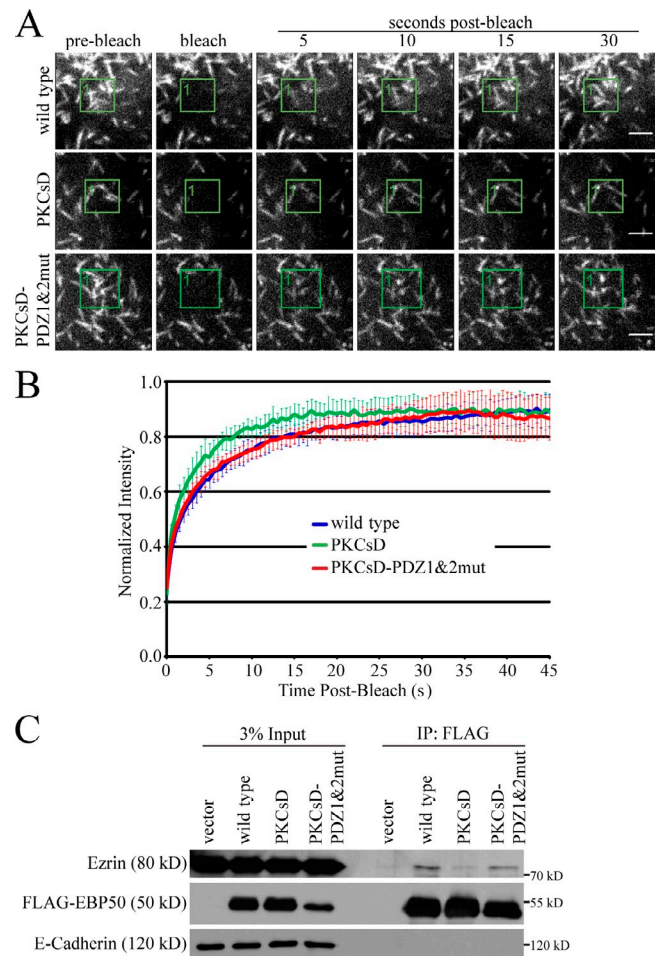
Figure 4. **PKC phosphorylation of EBP50 enhances its microvillar turnover.** (A) Time points from photobleaching experiments of GFP-tagged EBP50 wild type, PKCsD, and PKCsD-PDZ1&2 mutant (mut). Photobleached regions are shown as green boxes. Bars, 2 µm. (B) Recovery curves of GFP-EBP50 (n = 13), PKCsD (n = 10), and PKCsD-PDZ1&2 mutant (n = 11; wild type vs. PKCsD, P < 0.0001; wild type vs. PKCsD-PDZ1&2mut, P = 0.36). Error bars show SD. (C) 3xFLAG-tagged constructs of EBP50 constructs expressed in JEG-3 cells were immunoprecipitated (IP) and blotted for FLAG, endogenous ezrin, and E-cadherin as a control.

untagged EBP50 as a competitor, beads were withdrawn at various times and washed, and the amount of PAGFP-EBP50 remaining was determined (Fig. S2 A). This revealed that in vitro, PAGFP-EBP50 binds tenaciously to the ezrin FERM domain, with an off-rate best fit by a single exponential decay curve with a half-life of ∼21 min (Fig. S2 B). This contrasts with the in vivo dynamics of EBP50 associating with active ezrin for just a few seconds, which was best fit by a double exponential decay curve.

With this large difference between the in vivo and in vitro off-rates seen using different experimental procedures, we set out to develop an in vitro assay that more accurately reflects the in vivo situation. To mimic the open activated form of ezrin enriched in microvilli, ezrin FERM domain was covalently linked to 2-µm-diameter beads at a final bound concentration of 600 nM. The beads were then incubated with 7 µM recombinant PAGFP-EBP50 to saturate the immobilized ezrin FERM and mounted on coverslips. The beads were found by differential interference contrast, and the PAGFP-EBP50 bound to the FERM beads was
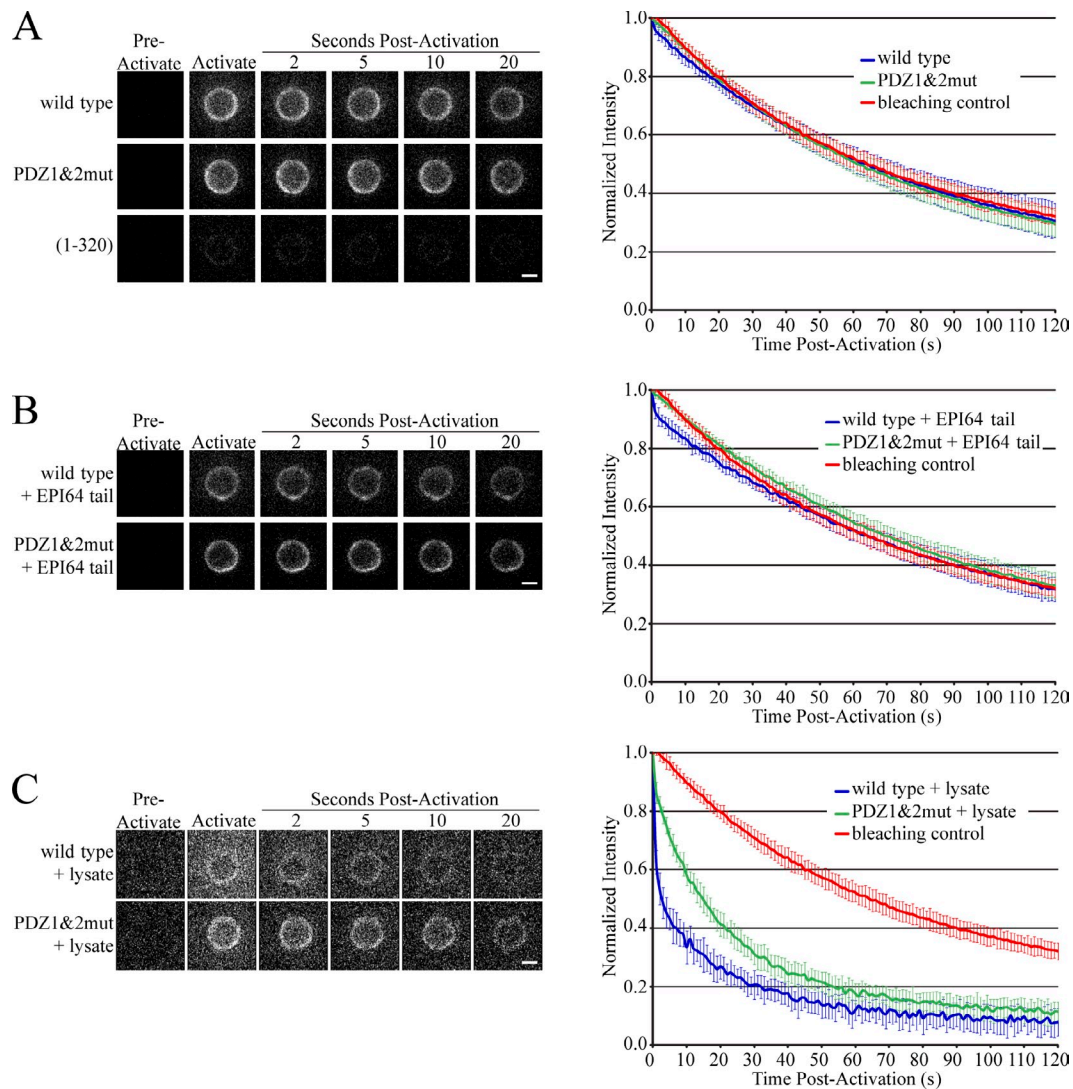
Figure 5. **The EBP50–ezrin interaction is stable in vitro but becomes dynamic upon addition of cell lysate.** (A, left) Time points from in vitro photoactivation experiments of PAGFP-tagged EBP50 constructs to determine their intrinsic off-rate from ezrin FERM coupled to 2-μm beads. mut, mutant. (right) Graph of the photoactivation decay curves of PAGFP-tagged EBP50 wild type ($n = 22$) and PDZ1&2 mutant ($n = 17$). The photobleaching control was PAGFP-EBP50 (1–320) covalently linked to beads ($n = 18$). Error bars indicate SD. (B) Same as A but with addition of 40 μM EPI64 tail (481–508) to the reaction (wild type, $n = 15$; PDZ1&2 mutant, $n = 13$). (C) Same as A but with addition of 2.8 mg/ml JEG-3 cell lysate (wild type, $n = 9$; PDZ1&2 mutant, $n = 15$). Bars, 1 μm.

selectively photoactivated with UV light. The decay in bead-associated fluorescence was monitored and reflected the dissociation of activated PAGFP-EBP50 and its replacement by nonactivated PAGFP-EBP50. This in vitro photoactivation method provides the benefit of being able to monitor off-rates continuously and on the same time scale as the in vivo experiments, without the need for time-consuming wash steps, which also disrupt the assay equilibrium.

To validate the assay, we first used PAGFP-EBP50(1–320) that lacks the C-terminal ezrin-binding site. Immediately after activation, no fluorescence could be detected (Fig. 5 A). To define the rate of photobleaching during the assay, we covalently coupled PAGFP-EBP50(1–320) to the beads and determined a bleaching curve. Having established these parameters, we followed the dissociation of PAGFP-EBP50 and the double PDZ1&2 mutant of PAGFP-EBP50 over a 120-s time frame.

All constructs remained firmly attached to the beads, losing fluorescence at a rate indistinguishable from the covalently bound PAGFP-EBP50(1–320) control (Fig. 5 A). To see whether ligand occupation of PDZ1 affected the off-rate, we repeated the assay in the presence of excess EPI64 tail, which binds with high affinity to PDZ1 (Reczek and Bretscher, 2001). An extremely minor, but reproducible, enhancement of the off-rate was seen (Fig. 5 B) but clearly not of the magnitude to explain the dynamics seen in vivo.

To explore whether cell extracts contain components that can enhance the PAGFP-EBP50 off-rates, we repeated the experiments in the presence of increasing concentrations of JEG-3 cell extract. For both PAGFP-EBP50 wild type and the PDZ1&2 double mutant, increasing concentrations of cell extract enhanced the off-rate (Fig. S3 A), but the off-rate was unaffected by a high concentration of bacterial extract and was not dependent on ATP

levels in JEG-3 cell lysate (Fig. S3, B and C). Remarkably, the JEG-3 cell extract enhanced the off-rate for wild-type PAGFP-EBP50 to a level similar to that seen in vivo (Fig. 5 C). Additionally, although the extract enhanced the off-rate for the PDZ1&2 double mutant, the enhancement was much less than for the wild-type protein, reflecting the same phenomenon we documented in vivo (Fig. 5 C). Therefore, our in vitro results confirm that the binary ezrin–EBP50 interaction is of high affinity with a slow off-rate that can be greatly enhanced by the presence of eukaryotic, but not prokaryotic, cell extracts in a PDZ-dependent manner.

Summary

The findings presented here represent an altered appreciation of the roles of scaffolding proteins. The name suggests that they bridge other proteins by making stable interactions, yet, here, we show that a scaffolding protein that is necessary for the assembly of a cell surface structure with a lifetime of several minutes can be exceptionally short lived, turning over in several seconds. A similar type of unexpected dynamics was reported for α-catenin in epithelial cells junctions: this linking protein is highly dynamic in a structure that is viewed as quite stable (Drees et al., 2005; Yamada et al., 2005). Additionally, the actin filament–cross-linking protein fascin shows rapid turnover from filopodia on a similar time scale as EBP50, but its dynamic nature is an intrinsic feature of its association with actin and can be fully recapitulated in vitro (Aratyn et al., 2007). In the case of EBP50, the relevance and function of these dynamics are unknown but perhaps are a reflection of both its diversity of interaction partners and roles in surface retention, trafficking, recycling, and signaling pathways (Weinman et al., 2006; Ardura and Friedman, 2011). Indeed, EBP50 also undergoes allosteric interdomain motion over submicrosecond time scales that are thought to play an important role in regulating formation of multiprotein complexes and subsequent signaling events (Farago et al., 2010).

We also find it quite remarkable that such a dynamic protein can participate in the localization of membrane proteins, such as PCX, to microvilli and exclusion from the primary cilium (Francis et al., 2011). How can EBP50 function amid such molecular turmoil? One possibility is that the overall number of EBP50's PDZ ligands in the membrane may create multiple rapid linkages to ezrin and is sufficient to retain them in the microvilli. This doesn't fully explain why the turnover is enhanced by ligands binding EBP50's PDZ domains. One potential answer would be that an increased number of PDZ ligands in microvilli would create increased turnover of EBP50 to regulate the amount of EBP50 bound to ezrin in a microvillus as a type of biological governor. To fully address this will require identification of the factors that enhance EBP50's dynamics, a task we are currently undertaking.

Materials and methods

Antibodies

Rabbit antisera against full-length human ezrin was previously described (Bretscher, 1989). The mouse anti–FLAG M2 and mouse anti–E-cadherin antibodies were purchased from Sigma-Aldrich and BD, respectively. Rabbit anti-tRFP (used against TagRFPT) was purchased from Axxora. Goat anti–rabbit and –mouse secondary antibodies conjugated to HRP were purchased from MP Biomedicals and Jackson ImmunoResearch Laboratories, Inc., respectively.

DNA constructs

N-terminal GFP and SUMO-tagged EBP50 constructs were created in pEGFP-C2 (Takara Bio Inc.) and pE-SUMO (LifeSensors, Inc.), respectively, and were previously described (Garbett et al., 2010). GFP-tagged ezrin and TROP2 were cloned into pEGFP-N2 (Takara Bio Inc.). N-terminally tagged GFP-PCX in pcDNA3, provided by D. Bryant and K. Mostov (University of California, San Francisco, San Francisco, CA), was previously described (Meder et al., 2005). TagRFPT-EBP50 constructs were created by PCR from a vector expressing TagRFPT that was provided by R. Tsien (University of California, San Diego, La Jolla, CA; Shaner et al., 2008). PAGFP fusions of EBP50 and ezrin were generated by restriction digest from PAGFP-C1, which was provided by J. Lippincott-Schwartz (National Institutes of Health, Bethesda, MD; Patterson and Lippincott-Schwartz, 2002). 3xFLAG-tagged EBP50 constructs were created using PCR and inserted into pQCXIP (BD). Untagged ezrin FERM (residues 1–298) in pQE16 (QIAGEN) was previously described (Reczek et al., 1997). The EPI64 tail residues 481–508 were inserted into pGEX-6P1 (GE Healthcare) using PCR and were previously described (Hokanson and Bretscher, 2012). DG-TagRFPT–EPI64 tail and the LA mutant were generated in two steps by PCR of DG for TagRFPT tagging followed by PCR of EPI64 tail or EPI64–LA tail residues 451–508 and inserted after the end of TagRFPT by restriction digest.

Cell culture and transfection

JEG-3 cells (American Type Culture Collection) were maintained in a 5% CO_2 humidified atmosphere at 37°C in MEM with 10% FBS (Invitrogen). Cells were transfected with polyethylenimine (Polysciences, Inc.) and 1–2 µg of plasmid DNA, as previously described (Hanono et al., 2006).

Purification of recombinant proteins

Ezrin FERM was purified as previously described (Reczek et al., 1997). In brief, induced cells were suspended in 180 mM KH_2PO_4, pH 7.0, with complete protease inhibitor (Roche), lysed by sonication (Branson Ultrasonics), centrifuged and run over a hydroxyapatite column (Pall Corporation), and eluted by a linear gradient of 180–800 mM KH_2PO_4, pH 7.0. Ezrin FERM–containing fractions were pooled and dialyzed against 20 mM MES (2-(N-morpholino)ethanesulfonic acid) and 150 mM NaCl, pH 6.7, and applied to an S-Sepharose column (GE Healthcare) and eluted in a linear gradient of 0.15–1.0 M NaCl. For conjugation of purified FERM to cyanogen bromide (CNBr)–activated Sepharose (Sigma-Aldrich), FERM was dialyzed into C buffer (0.1 M $NaHCO_3$ and 0.5 M NaCl, pH 8.3) and then added overnight to hydrated CNBr beads for a final concentration of 38.5 µM on the resin. Beads were then washed and blocked in 0.25 M glycine, pH 8.0, overnight. Beads were then washed again and stored as a 50% slurry in H buffer (50 mM Tris and 150 mM NaCl, pH 7.4). For conjugation of FERM to 2-µm carboxylated polystyrene microspheres (Polysciences, Inc.), 1 mg of FERM was added to 12.5 mg of microspheres and coupled using the PolyLink protein coupling kit instructions (Polysciences, Inc.) with an additional block using 5% low–molecular weight dextran in 0.25 M glycine, pH 8.0. The final concentration of FERM covalently coupled to the microspheres was 200 µM.

Bacterial pellets induced to express either GST–EPI64 tail (481–508) or GST–3CPro protease were lysed in 150 mM NaCl, 20 mM Tris, 0.1% β-mercaptoethanol, and 0.1% Triton X-100, pH 7.4, with complete protease inhibitor by sonication, centrifuged and added to hydrated glutathione agarose (Sigma-Aldrich), washed, and then mixed together overnight at 4°C to cleave the EPI64 tail off the beads.

SUMO-PAGFP-EBP50 constructs were purified as previously described (LaLonde et al., 2010), but all steps were performed in the dark to minimize background activation of PAGFP. In brief, induced bacterial pellets were lysed in binding buffer (20 mM sodium phosphate, 500 mM NaCl, 20 mM imidazole, and 1% Triton X-100, pH 7.4) by sonication, centrifuged and run over a His gravitrap column (GE Healthcare), washed, and eluted in elution buffer (20 mM sodium phosphate, 500 mM NaCl, and 500 mM imidazole, pH 7.4). Eluate was dialyzed into binding buffer, cleaved with 6xHis-Ulp1 for 40 min at 30°C to remove the SUMO tag, and then run over another His gravitrap column, and flow-through containing PAGFP-EBP50 was collected and dialyzed into 20 mM Hepes and 300 mM NaCl, pH 7.4.

Live-cell imaging, FRAP, and photoactivation

Transfected JEG-3 cells grown in 35-mm glass-bottom dishes (MatTek Corporation) were washed twice in PBS and then maintained in low–sodium

bicarbonate phenol red–free MEM (Sigma-Aldrich) supplemented with 25 mM Hepes, pH 7.4, with 10% FBS and GlutaMAX (Invitrogen). Live cells were imaged by time-lapse microscopy on a spinning disk (CSU-X; Intelligent Imaging Innovations, Inc.) with a spherical aberration correction device, a 100× 1.46 NA objective (Leica) on an inverted microscope (DMI6000B; Leica), and an electron-multiplied charge-coupled device camera (QuantEM; Photometrics) at 37°C in an environmental chamber (Okolab) controlled by SlideBook (v5.0; Intelligent Imaging Innovations, Inc.). Regions selected for FRAP and photoactivation were illuminated using a digital mirror illumination system (Mosaic; Andor Technology) coupled to either a 488-nm 400W argon laser or mercury light source (Carl Zeiss) running through a 405-nm excitation filter, respectively. For all FRAP experiments, an independent region was also monitored to control for photobleaching during the observation period. Videos were processed using SlideBook (v5.0) and analyzed using ImageJ (National Institutes of Health), Excel (Microsoft), and Prism (GraphPad Software). Expression levels of cells were determined by GFP fluorescence, and FRAP recoveries of cells with varying expression levels were compared to ensure that differences in recovery rates were not a result of expression variation. The normalized data from multiple biological replicates were fit with a curve, and samples with overlapping SD were subjected to a two-way analysis of variance using Prism.

Immunoprecipitation and Western blotting
JEG-3 cells transiently expressing 3xFLAG-EBP50 constructs were lysed in lysis buffer (25 mM Tris, 150 mM NaCl, 1% IGEPAL-630, 50 mM NaF, 0.1 mM Na_3VO_4, 10 mM β-GP, and 2.5% glycerol, pH 7.4) and incubated with anti–FLAG M2 affinity resin (Sigma-Aldrich) while nutating at 4°C for 2 h. The resin was then washed three times in lysis buffer with 0.1% IGEPAL-630, and the remaining bound sample was eluted using 3xFLAG peptide (Sigma-Aldrich) for 45 min at room temperature. Protein samples were boiled in sample buffer and separated by SDS-PAGE and transferred to Immobilon-P (EMD Millipore) for Western blotting and then visualized using ECL (GE Healthcare).

In vitro competition assay
Excess ezrin FERM domain coupled to CNBr beads at a final concentration of 240 nM was mixed with 40 nM of soluble PAGFP-EBP50 in 300 mM NaCl, 0.1% Triton X-100, 5% glycerol, and 20 mM Tris, pH 7.4, and nutated for 1 h at 4°C. Beads were spun and quickly washed once, and then buffer containing excess untagged EBP50 at 1 µM was added for the various times indicated to compete with the prebound PAGFP-EBP50. Beads were spun, quickly washed, and then boiled in sample buffer and separated by SDS-PAGE. The gel was stained with IRDye (LI-COR Biosciences) and then imaged and analyzed using an infrared imaging system (Odyssey; LI-COR Biosciences). The normalized data were fit to a curve using Prism.

In vitro photoactivation assay
Ezrin FERM coupled to 2-µm beads at a final concentration of 600 nM was added to excess PAGFP-EBP50 constructs at 7 µM in 20 mM Hepes, 300 mM NaCl, and 1% polyethylene glycol, pH 7.4. Experiments that included EPI64 tail contained it at 40 µM, and experiments using JEG-3 cell or bacterial lysate used it at a final concentration of 2.4 mg/ml unless otherwise indicated. To deplete ATP, JEG-3 cell lysate was treated with 1 U apyrase (Sigma-Aldrich) per 20 µl of lysate on ice for 30 min. To regenerate ATP, JEG-3 cell lysate was treated with 5 U of creatine phosphokinase (Sigma-Aldrich) per 20 µl of lysate with 10 mM phosphocreatine di-Tris salt (Sigma-Aldrich) at 30°C for 30 min. ATP levels were verified by colorimetric assay (BioVision, Inc.). The reaction mixture was added to a glass coverslip and affixed to a glass slide using VALAP (a mixture of vaseline, lanolin, and paraffin). Beads were imaged by time-lapse microscopy on a spinning disk (CSU-X) with a spherical aberration correction device, a 100× 1.46 NA objective on an inverted microscope (DMI6000B), and an electron-multiplied charge-coupled device camera (QuantEM) controlled by SlideBook (v5.0). Beads were found by differential interference contrast, and the corresponding regions were photoactivated using a digital mirror illumination system (Mosaic) coupled to a mercury light source (Carl Zeiss) running through a 405-nm excitation filter. Videos were processed using SlideBook (v5.0) and analyzed using Excel and Prism.

Online supplemental material
Fig. S1 shows quantification of microvilli lengths over time and the recovery rate fitting of FRAP data in Fig. 1. Fig. S2 shows that EBP50 stably associates with ezrin FERM domain in vitro. Fig. S3 shows in vitro photoactivation assays examining the effects on the off-rate of EBP50 from ezrin FERM with increasing JEG-3 cell lysate concentrations, addition of bacterial lysate, and independence on ATP levels. Online supplemental material is available at http://www.jcb.org/cgi/content/full/jcb.201204008/DC1.

References

Aratyn, Y.S., T.E. Schaus, E.W. Taylor, and G.G. Borisy. 2007. Intrinsic dynamic behavior of fascin in filopodia. *Mol. Biol. Cell.* 18:3928–3940. http://dx.doi.org/10.1091/mbc.E07-04-0346

Ardura, J.A., and P.A. Friedman. 2011. Regulation of G protein-coupled receptor function by Na+/H+ exchange regulatory factors. *Pharmacol. Rev.* 63:882–900. http://dx.doi.org/10.1124/pr.110.004176

Ardura, J.A., B. Wang, S.C. Watkins, J.P. Vilardaga, and P.A. Friedman. 2011. Dynamic Na+-H+ exchanger regulatory factor-1 association and dissociation regulate parathyroid hormone receptor trafficking at membrane microdomains. *J. Biol. Chem.* 286:35020–35029. http://dx.doi.org/10.1074/jbc.M111.264978

Bretscher, A. 1989. Rapid phosphorylation and reorganization of ezrin and spectrin accompany morphological changes induced in A-431 cells by epidermal growth factor. *J. Cell Biol.* 108:921–930. http://dx.doi.org/10.1083/jcb.108.3.921

Chen, J.Y., Y.Y. Lin, and T.S. Jou. 2012. Phosphorylation of EBP50 negatively regulates β-PIX-dependent Rac1 activity in anoikis. *Cell Death Differ.* 19:1027–1037. http://dx.doi.org/10.1038/cdd.2012.4

Coscoy, S., F. Waharte, A. Gautreau, M. Martin, D. Louvard, P. Mangeat, M. Arpin, and F. Amblard. 2002. Molecular analysis of microscopic ezrin dynamics by two-photon FRAP. *Proc. Natl. Acad. Sci. USA.* 99:12813–12818. http://dx.doi.org/10.1073/pnas.192084599

Drees, F., S. Pokutta, S. Yamada, W.J. Nelson, and W.I. Weis. 2005. Alpha-catenin is a molecular switch that binds E-cadherin-beta-catenin and regulates actin-filament assembly. *Cell.* 123:903–915. http://dx.doi.org/10.1016/j.cell.2005.09.021

Farago, B., J. Li, G. Cornilescu, D.J. Callaway, and Z. Bu. 2010. Activation of nanoscale allosteric protein domain motion revealed by neutron spin echo spectroscopy. *Biophys. J.* 99:3473–3482. http://dx.doi.org/10.1016/j.bpj.2010.09.058

Fehon, R.G., A.I. McClatchey, and A. Bretscher. 2010. Organizing the cell cortex: The role of ERM proteins. *Nat. Rev. Mol. Cell Biol.* 11:276–287. http://dx.doi.org/10.1038/nrm2866

Fouassier, L., M.T. Nichols, E. Gidey, R.R. McWilliams, H. Robin, C. Finnigan, K.E. Howell, C. Housset, and R.B. Doctor. 2005. Protein kinase C regulates the phosphorylation and oligomerization of ERM binding phosphoprotein 50. *Exp. Cell Res.* 306:264–273. http://dx.doi.org/10.1016/j.yexcr.2005.02.011

Francis, S.S., J. Sfakianos, B. Lo, and I. Mellman. 2011. A hierarchy of signals regulates entry of membrane proteins into the ciliary membrane domain in epithelial cells. *J. Cell Biol.* 193:219–233. http://dx.doi.org/10.1083/jcb.201009001

Garbett, D., D.P. LaLonde, and A. Bretscher. 2010. The scaffolding protein EBP50 regulates microvillar assembly in a phosphorylation-dependent manner. *J. Cell Biol.* 191:397–413. http://dx.doi.org/10.1083/jcb.201004115

Gorelik, J., A.I. Shevchuk, G.I. Frolenkov, I.A. Diakonov, M.J. Lab, C.J. Kros, G.P. Richardson, I. Vodyanoy, C.R. Edwards, D. Klenerman, and Y.E. Korchev. 2003. Dynamic assembly of surface structures in living cells. *Proc. Natl. Acad. Sci. USA.* 100:5819–5822. http://dx.doi.org/10.1073/pnas.1030502100

Hanono, A., D. Garbett, D. Reczek, D.N. Chambers, and A. Bretscher. 2006. EPI64 regulates microvillar subdomains and structure. *J. Cell Biol.* 175:803–813. http://dx.doi.org/10.1083/jcb.200604046

Hokanson, D.E., and A.P. Bretscher. 2012. EPI64 interacts with Slp1/JFC1 to coordinate Rab8a and Arf6 membrane trafficking. *Mol. Biol. Cell.* 23:701–715. http://dx.doi.org/10.1091/mbc.E11-06-0521

LaLonde, D.P., D. Garbett, and A. Bretscher. 2010. A regulated complex of the scaffolding proteins PDZK1 and EBP50 with ezrin contribute to microvillar

organization. *Mol. Biol. Cell.* 21:1519–1529. http://dx.doi.org/10.1091/mbc.E10-01-0008

Lippincott-Schwartz, J., and G.H. Patterson. 2009. Photoactivatable fluorescent proteins for diffraction-limited and super-resolution imaging. *Trends Cell Biol.* 19:555–565. http://dx.doi.org/10.1016/j.tcb.2009.09.003

Loomis, P.A., L. Zheng, G. Sekerková, B. Changyaleket, E. Mugnaini, and J.R. Bartles. 2003. Espin cross-links cause the elongation of microvillus-type parallel actin bundles in vivo. *J. Cell Biol.* 163:1045–1055. http://dx.doi.org/10.1083/jcb.200309093

Meder, D., A. Shevchenko, K. Simons, and J. Füllekrug. 2005. Gp135/podocalyxin and NHERF-2 participate in the formation of a preapical domain during polarization of MDCK cells. *J. Cell Biol.* 168:303–313. http://dx.doi.org/10.1083/jcb.200407072

Patterson, G.H., and J. Lippincott-Schwartz. 2002. A photoactivatable GFP for selective photolabeling of proteins and cells. *Science*. 297:1873–1877. http://dx.doi.org/10.1126/science.1074952

Raghuram, V., H. Hormuth, and J.K. Foskett. 2003. A kinase-regulated mechanism controls CFTR channel gating by disrupting bivalent PDZ domain interactions. *Proc. Natl. Acad. Sci. USA*. 100:9620–9625. http://dx.doi.org/10.1073/pnas.1633250100

Reczek, D., and A. Bretscher. 1998. The carboxyl-terminal region of EBP50 binds to a site in the amino-terminal domain of ezrin that is masked in the dormant molecule. *J. Biol. Chem.* 273:18452–18458. http://dx.doi.org/10.1074/jbc.273.29.18452

Reczek, D., and A. Bretscher. 2001. Identification of EPI64, a TBC/rabGAP domain–containing microvillar protein that binds to the first PDZ domain of EBP50 and E3KARP. *J. Cell Biol.* 153:191–206. http://dx.doi.org/10.1083/jcb.153.1.191

Reczek, D., M. Berryman, and A. Bretscher. 1997. Identification of EBP50: A PDZ-containing phosphoprotein that associates with members of the ezrin-radixin-moesin family. *J. Cell Biol.* 139:169–179. http://dx.doi.org/10.1083/jcb.139.1.169

Romero, G., M. von Zastrow, and P.A. Friedman. 2011. Role of PDZ proteins in regulating trafficking, signaling, and function of GPCRs: Means, motif, and opportunity. *Adv. Pharmacol.* 62:279–314. http://dx.doi.org/10.1016/B978-0-12-385952-5.00003-8

Shaner, N.C., M.Z. Lin, M.R. McKeown, P.A. Steinbach, K.L. Hazelwood, M.W. Davidson, and R.Y. Tsien. 2008. Improving the photostability of bright monomeric orange and red fluorescent proteins. *Nat. Methods*. 5:545–551. http://dx.doi.org/10.1038/nmeth.1209

Spence, H.J., Y.J. Chen, C.L. Batchelor, J.R. Higginson, H. Suila, O. Carpen, and S.J. Winder. 2004. Ezrin-dependent regulation of the actin cytoskeleton by beta-dystroglycan. *Hum. Mol. Genet.* 13:1657–1668. http://dx.doi.org/10.1093/hmg/ddh170

Terawaki, S., R. Maesaki, and T. Hakoshima. 2006. Structural basis for NHERF recognition by ERM proteins. *Structure*. 14:777–789.

Tyska, M.J., and M.S. Mooseker. 2002. MYO1A (brush border myosin I) dynamics in the brush border of LLC-PK1-CL4 cells. *Biophys. J.* 82:1869–1883. http://dx.doi.org/10.1016/S0006-3495(02)75537-9

Waharte, F., C.M. Brown, S. Coscoy, E. Coudrier, and F. Amblard. 2005. A two-photon FRAP analysis of the cytoskeleton dynamics in the microvilli of intestinal cells. *Biophys. J.* 88:1467–1478. http://dx.doi.org/10.1529/biophysj.104.049619

Weinman, E.J., D. Steplock, Y. Wang, and S. Shenolikar. 1995. Characterization of a protein cofactor that mediates protein kinase A regulation of the renal brush border membrane Na(+)-H+ exchanger. *J. Clin. Invest.* 95:2143–2149. http://dx.doi.org/10.1172/JCI117903

Weinman, E.J., R.A. Hall, P.A. Friedman, L.Y. Liu-Chen, and S. Shenolikar. 2006. The association of NHERF adaptor proteins with g protein-coupled receptors and receptor tyrosine kinases. *Annu. Rev. Physiol.* 68:491–505. http://dx.doi.org/10.1146/annurev.physiol.68.040104.131050

Yamada, S., S. Pokutta, F. Drees, W.I. Weis, and W.J. Nelson. 2005. Deconstructing the cadherin-catenin-actin complex. *Cell*. 123:889–901. http://dx.doi.org/10.1016/j.cell.2005.09.020

Yu, C.Y., J.Y. Chen, Y.Y. Lin, K.F. Shen, W.L. Lin, C.L. Chien, M.B. ter Beest, and T.S. Jou. 2007. A bipartite signal regulates the faithful delivery of apical domain marker podocalyxin/Gp135. *Mol. Biol. Cell*. 18:1710–1722. http://dx.doi.org/10.1091/mbc.E06-07-0629